Title

Mechanism of scrapie prion precipitation with phosphotungstate anions.

Journal

ACS Chemical Biology, 10(5)

Authors

Levine, Dana

Stöhr, Jan

Falese, Lillian

et al.

Publication Date

2015-05-15

DOI

10.1021/cb5006239

Peer reviewed

ACS chemical biology

Articles

pubs.acs.org/acschemicalbiology

Mechanism of Scrapie Prion Precipitation with Phosphotungstate Anions

Dana J. Levine,[†,‡] Jan Stöhr,[‡,§] Lillian E. Falese,[‡] Julian Ollesch,[‡,⊥] Holger Wille,[‡,§,∥] Stanley B. Prusiner,[‡,§] and Jeffrey R. Long*[,†]

[†]Department of Chemistry, University of California, Berkeley, 211 Lewis Hall, Berkeley, California 94720, United States

[‡]Institute for Neurodegenerative Diseases, University of California, San Francisco, 675 Nelson Rising Lane, San Francisco, California 94143, United States

[§]Department of Neurology, University of California, San Francisco, 675 Nelson Rising Lane, San Francisco, California 94143, United States

Supporting Information

ABSTRACT: The phosphotungstate anion (PTA) is widely used to facilitate the precipitation of disease-causing prion protein (PrP^{Sc}) from infected tissue for applications in structural studies and diagnostic approaches. However, the mechanism of this precipitation is not understood. In order to elucidate the nature of the PTA interaction with PrP^{Sc} under physiological conditions, solutions of PTA were characterized by NMR spectroscopy at varying pH. At neutral pH, the parent $[PW_{12}O_{40}]^{3-}$ ion decomposes to give a lacunary $[PW_{11}O_{39}]^{7-}$ (PW_{11}) complex and a single orthotungstate anion $[WO_4]^{2-}$ (WO_4). To measure the efficacy of each component of PTA, increasing concentrations of PW_{11}, WO_4, and mixtures thereof were used to precipitate PrP^{Sc} from brain homogenates of scrapie prion-infected mice. The amount of PrP^{Sc} isolated, quantified by ELISA and immunoblotting, revealed that both PW_{11} and WO_4 contribute to PrP^{Sc} precipitation. Incubation with sarkosyl, PTA, or individual components of PTA resulted in separation of higher-density PrP aggregates from the neuronal lipid monosialotetrahexosylganglioside (GM1), as observed by sucrose gradient centrifugation. These experiments revealed that yield and purity of PrP^{Sc} were greater with polyoxometalates (POMs), which substantially supported the separation of lipids from PrP^{Sc} in the samples. Interaction of POMs and sarkosyl with brain homogenates promoted the formation of fibrillar PrP^{Sc} aggregates prior to centrifugation, likely through the separation of lipids like GM1 from PrP^{Sc}. We propose that this separation of lipids from PrP is a major factor governing the facile precipitation of PrP^{Sc} by PTA from tissue and might be optimized further for the detection of prions.

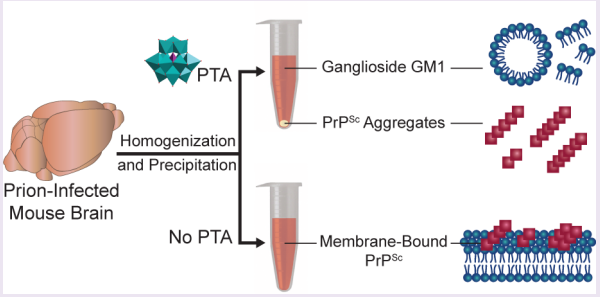

The fundamental event in prion diseases caused by the prion protein (PrP) is the misfolding of normal PrP (PrP^{C}), which leads to progressive neurodegeneration in many mammals.[1] Such diseases include Creutzfeldt–Jakob disease in humans, scrapie in sheep, bovine spongiform encephalopathy in cattle, and chronic wasting disease in deer and elk.[2] In these prion diseases, endogenous PrP^{C} adopts a self-propagating conformation, designated PrP^{Sc}, which can autocatalytically convert PrP^{C} molecules into infectious PrP^{Sc}.[3,4] PrP misfolding can be caused by genetic mutations, exposure to PrP^{Sc}, or occur spontaneously, resulting in inherited, acquired, or sporadic disease manifestations, respectively.[5] Over time, PrP^{Sc} accumulates and spreads throughout the brain, leading to severe neuronal deterioration, loss of cognitive function, and ultimately death. While diseases caused by PrP^{Sc} are rare in humans, biochemical insights into PrP^{Sc} may provide valuable applications to other, more common neurodegenerative disorders. In recent studies, a self-perpetuating prion mechanism has been described for amyloid β peptides in Alzheimer's disease, α-synuclein in Parkinson's disease, and tau in the tauopathies.[6−11]

A detailed knowledge of the structure of PrP^{Sc} would greatly facilitate efforts to prevent, diagnose, and develop therapeutics for prion diseases. PrP^{Sc} is rich in β-sheet content that renders the large aggregates insoluble and thus difficult to characterize by conventional biophysical techniques. Despite studies employing X-ray fiber diffraction,[12] electron microscopy,[13] and hydrogen−deuterium exchange,[14] the structure of PrP^{Sc} remains elusive. Structural models of PrP^{Sc} have been proposed from X-ray fiber diffraction and electron microscopy of prions isolated from brain tissue.[12,15] However, such fibril preparations generally contain large amounts of crystalline lipids, which may obscure structural features of the protein aggregates.

Received: August 5, 2014
Accepted: November 25, 2014
Published: November 25, 2014

DOI: 10.1021/cb5006239
ACS Chem. Biol. 2015, 10, 1269−1277

Biophysical studies require the purification of a relatively large amount of PrP^{Sc}. Historically, prion purification and enrichment required a series of time-intensive gradient or differential centrifugation steps, which resulted in highly purified samples but with a low yield.[16−18] A rapid, alternative method employs an inorganic polyoxometalate (POM) complex known as the phosphotungstate anion (PTA, $[PW_{12}O_{40}]^{3-}$). Since the discovery that PTA selectively promotes precipitation of PrP^{Sc} over PrP^{C},[19] it has been widely used to isolate PrP^{Sc} from various tissues of prion-infected animals.[20−25] The success of PTA has stimulated efforts to vary the structure, charge, and composition of related complexes to optimize PrP^{Sc} purification[26] and to influence the resulting type of aggregate assemblies.[15]

PTA precipitation has also been used to concentrate PrP^{Sc} for diagnostic purposes.[27,28] Currently, a definitive diagnosis of prion diseases caused by PrP^{Sc} can only be made post-mortem. Efforts have been made to develop diagnostic tools for detecting PrP^{Sc} in the blood of humans and cattle,[29,30] and PTA has been used to facilitate detection of very low amounts of PrP^{Sc} in peripheral tissues of patients with Creutzfeldt−Jakob disease.[31] However, achieving a rapid and reliable method for PrP^{Sc} detection has been hampered by difficulties in discriminating infectious PrP^{Sc} from endogenous PrP^{C}, low titers of PrP^{Sc} in blood, and the presence of lipid and protein contaminants that can complicate the accuracy of determinations.[32]

Despite the widespread use of PTA to isolate PrP^{Sc}, the mechanisms by which PTA effectively precipitates PrP^{Sc} are still largely unknown. PTA does not appear to induce a conformational change of PrP^{C} to PrP^{Sc}, since amyloid seeding assays have shown that PTA does not promote conversion of PrP^{C} to PrP^{Sc} in multiple strains of uninfected mice.[28] Using microscopic and immunological techniques, we found that PTA and sarkosyl promoted the formation of fibrils and increased the density of PrP^{Sc} aggregates. $Na_3[PW_{12}O_{40}]$ (NaPTA) decomposed at neutral pH to give a lacunary $[PW_{11}O_{39}]^{7-}$ (PW_{11}) complex and a single orthotungstate $[WO_4]^{2-}$ unit (WO_4). When used as a precipitant, the lacunary PW_{11} complex of PTA resulted in high yields of PrP^{Sc} and decreased neuronal lipid monosialotetrahexosylganglioside (GM1) content in the samples, while WO_4 was less effective at removing GM1 lipids at equivalent concentrations. These results describe several potential mechanisms for the effective precipitation of PrP^{Sc} by PTA.

RESULTS AND DISCUSSION

PTA and Sarkosyl Promote Formation of PrP^{Sc} Fibrils. In the standard method to precipitate PrP^{Sc} using PTA, prion-infected brain homogenates are incubated with PTA and the detergent sodium lauryl sarcosinate (sarkosyl) in phosphate-buffered saline (PBS) prior to a low-speed centrifugation. To test the influence of each precipitant on the aggregation state of PrP^{Sc}, we incubated brain homogenates (10% w/v) from FVB mice infected with Rocky Mountain Laboratory (RML) scrapie prions with different concentrations of sarkosyl (0−3.5% w/v), PTA (0−3.4% w/v), and combinations of 0−3.4% PTA with 2% sarkosyl. These scrapie-infected mice generally do not show preformed PrP^{Sc} fibrils or amyloid deposits in their brains.[33] The resulting PrP^{Sc} fibrillar aggregates were analyzed by electron microscopy of sample aliquots and quantified (Figure 1a). When neither sarkosyl nor PTA was used, very few fibrils were observed (Figure 1b). When used independently, both

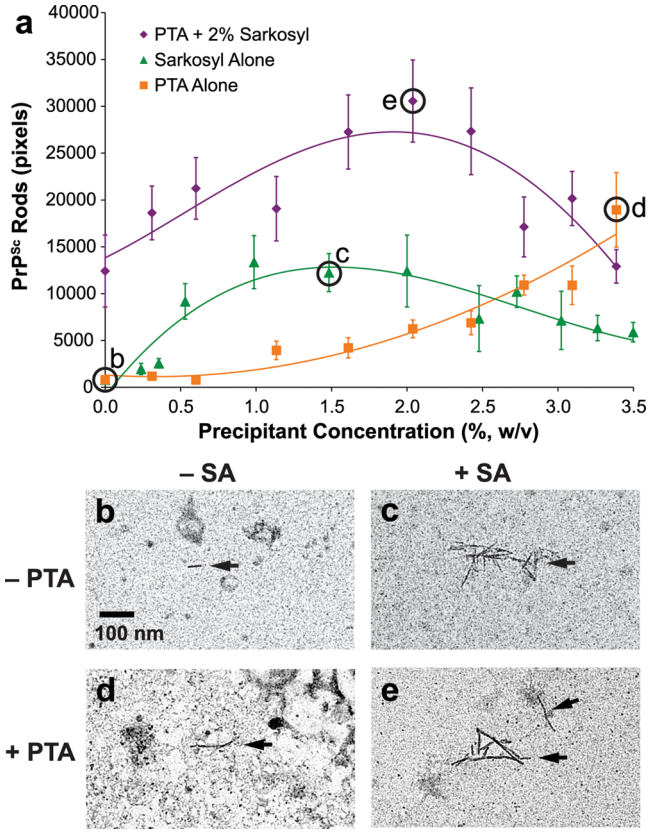

Figure 1. Quantification of electron microscopy images (a) shows how preparative methods with no additives (b), sarkosyl detergent alone (c), PTA alone (d), and PTA in combination with sarkosyl (e) influence the amount of PrP^{Sc} fibrils obtained at different reagent concentrations. Error bars in panel a represent the standard error of the mean from 10 representative electron micrographs, and examples of fibrils indicated by the letters in panel a are shown in panels b−e (arrows).

sarkosyl and PTA induced the formation of large fibrillar structures (Figure 1c,d, respectively). With PTA alone, higher concentrations yielded greater numbers of aggregates. The greatest number of fibrils detectable by electron microscopy was found from using a combination of PTA and sarkosyl, with the highest yield of fibrillar aggregates obtained using 2% PTA and 2% sarkosyl (Figure 1e), in agreement with established optimal concentrations from earlier studies.[12,15,26]

PTA Facilitates PrP^{Sc} Separation from Lipids. We further investigated the influence of PTA and sarkosyl on the hydrodynamic properties of aggregates by centrifugation of RML-infected brain homogenate in a three-step sucrose gradient. Brain homogenate (20% w/v) was prepared from RML-infected mice using PBS and 2% sarkosyl. The homogenate was then incubated at 37 °C overnight with or without 2% PTA, and then 1.5 mL of treated or untreated brain homogenate was loaded onto a sucrose gradient consisting of an 8 mL layer of 50% sucrose above a 2 mL layer of 80% sucrose. After centrifugation at 134 000*g* for 16 h, fractions from lowest to highest density were collected and immunoblotted for PrP levels and for GM1, the main ganglioside in neuronal membranes[34] and a marker for glycolipid raft domains[35,36] (Figure 2).

In the absence of PTA, PrP largely remained in fractions above the 50−80% sucrose interface, with most of the PrP settled at the interface of the aqueous buffer fraction and the

DOI: 10.1021/cb5006239
ACS Chem. Biol. 2015, 10, 1269−1277

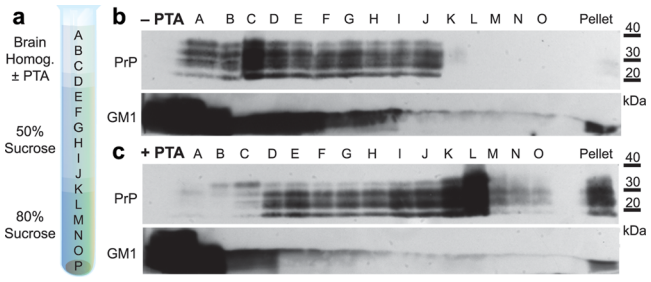

Figure 2. Sucrose cushion centrifugations of prion-infected brain homogenates reveal levels of PrP and GM1 by immunoblotting. (a) Schematic representation of the three-step gradient centrifugation, where the brain homogenate was layered on top of sucrose layers of increasing density. The resulting fractions were labeled A–P and correspond to lanes in the immunoblots. (b, c) Western blots of brain homogenate incubated without (b) or with (c) PTA. PrP (upper blots) and GM1 (lower blots) colocalized in the absence of PTA, whereas PrP separated from GM1 in the presence of PTA. Molecular weight markers of migrated protein standards are shown in kilodaltons (kDa).

first sucrose-containing fraction (Figure 2b, lanes C and D). In addition, the highest GM1 content was found to colocalize with PrP in the low-density fractions. This observation is consistent with the presence of a C-terminal glycophosphatidylinositol (GPI) anchor on PrP, which strongly interacts with lipids and increases the buoyancy of both monomeric PrP^{C} and aggregated PrP^{Sc}.[37,38] In the presence of PTA, PrP was found in higher density fractions, with the highest levels found below the 50–80% sucrose interface (Figure 2c, lanes K and L) and many aggregates clearly penetrating the 80% layer. With PTA, GM1 was also separated from the PrP aggregates, as evidenced by GM1 remaining in lower-density fractions while PrP migrated into higher-density fractions, even giving rise to a sizable amount of PrP in the pellet fraction. In this way, PTA also provided effective separation of monomeric PrP^{C} from aggregated PrP^{Sc}, since the buoyant PrP^{C} remained in the less dense GM1-containing fractions while aggregated PrP^{Sc} was more readily precipitated. This effect is further illustrated in samples treated with proteinase K (PK), which degrades PrP^{C} and cleaves PK-resistant PrP^{Sc} into PrP 27–30 (Supplementary Figure S1, Supporting Information). Without PTA, the majority of PrP 27–30 was found in the lower density fractions together with GM1 in proteolytically digested samples. Upon addition of PTA, however, PrP 27–30 migrated to the higher density fractions, effectively separating PrP from GM1 lipids, which remained in the low-density fractions.

PTA altered the distribution of PrP and GM1 in sucrose cushion centrifugations, suggesting that PTA may influence the density of PrP aggregates in several different ways. Direct interaction of PrP aggregates with heavy, tungsten-containing compounds like PTA may increase their density and promote the formation of larger PrP^{Sc} aggregates. In order to determine the effects of ionic strength on precipitation efficiency, sucrose

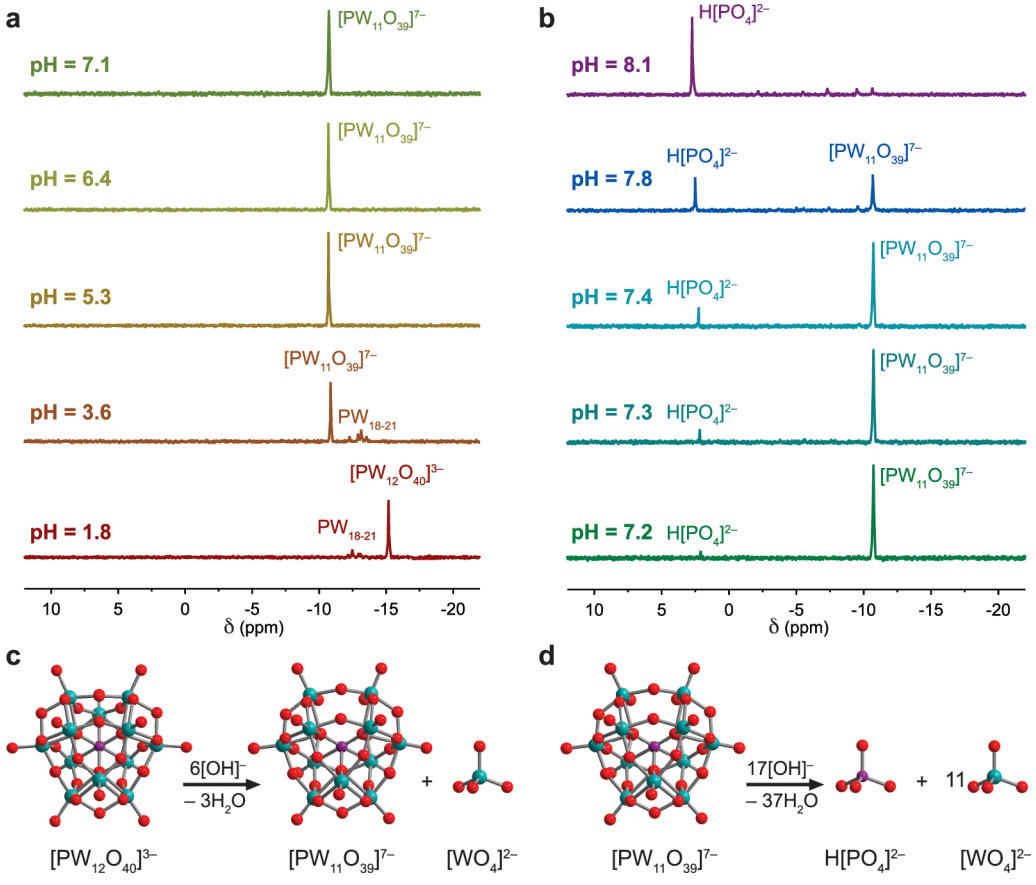

Figure 3. ^{31}P NMR demonstrates that PTA anion speciation changes dramatically with pH. (a, b) NMR spectra for acidic to neutral pH conditions (a) and for neutral to alkaline pH conditions (b). (c) Up to pH 7.0, the parent $[PW_{12}O_{40}]^{3-}$ ion decomposes to give a 1:1 mixture of $[PW_{11}O_{39}]^{7-}$ and $[WO_4]^{2-}$. (d) Above pH 7.1, the lacunary $[PW_{11}O_{39}]^{7-}$ ion begins to decompose into $H[PO_4]^{2-}$ and 11 $[WO_4]^{2-}$ complexes. Structural representations for $[PW_{12}O_{40}]^{3-}$, $[PW_{11}O_{39}]^{7-}$, and $[WO_4]^{2-}$ are from crystallographic information files found in refs 41, 60, and 61, respectively.

DOI: 10.1021/cb5006239
ACS Chem. Biol. 2015, 10, 1269–1277

cushion centrifugations were also performed on both PK-digested and undigested samples treated with sodium chloride (Supplementary Figure S2, Supporting Information). Addition of NaCl facilitated some degree of GM1 separation from PrP in both cases. However, NaCl did not significantly promote precipitation of PrP, suggesting that the efficacy of PTA may involve its direct interaction with PrP rather than simply increasing the ionic strength of the solution.

We speculate that the release of PrP from lipids is also a key factor in promoting fibrillization, as observed in the fibrillization studies using sarkosyl (Figure 1). Indeed, transgenic mice expressing PrP without the GPI anchor showed increased propensity to develop amyloid fibrils in their brains.[39,40] These observations suggest that interaction of PrP^{Sc} with lipid membranes may hinder fibril formation, and use of polyanions like PTA may aid in disrupting the membrane−PrP^{Sc} interaction to facilitate fibrillization of PrP^{Sc}, resulting in denser aggregates that are easier to precipitate than their lipid-bound counterparts.

Decomposition of PTA at Varying pH Studied by ^{31}P NMR. To further elucidate the mechanisms of the PTA precipitation, the POM speciation was determined under a range of conditions, particularly those typically used for PrP^{Sc} precipitation. Aqueous solutions of PTA at varying pH were studied by ^{31}P NMR (Figure 3). This technique is very useful in tracking changes in the POM composition because the chemical shift of the central phosphorus atom reflects its unique chemical environment and can be used to determine which species are present. PTA samples were also prepared in complex matrices by dissolving PTA in solutions containing PBS, sarkosyl, and brain tissue at pH 7, which confirmed that PTA speciation did not change in the presence of brain homogenate compared with a water-based solution (Supplementary Figure S3, Supporting Information). Furthermore, the speciation of PTA at neutral pH in water or brain homogenate did not change over the course of eight weeks, as observed by ^{31}P NMR (Supplementary Figure S4, Supporting Information).

PTA is synthesized by acidification of an aqueous solution containing stoichiometric amounts of tungstate and phosphate to give the product $[PW_{12}O_{40}]^{3-}$ (PW_{12}).[41] When this complex is used in biological contexts, the increase in pH from 1 to 7 leads to notable changes in the structure of the POM in solution.[42−44] By NMR spectroscopy, we confirmed that commercial $Na_3[PW_{12}O_{40}]$ (NaPTA) decomposed at neutral pH to give a lacunary $[PW_{11}O_{39}]^{7-}$ (PW_{11}) complex and a single orthotungstate $[WO_4]^{2-}$ unit (WO_4) in a 1:1 ratio (Figure 3a). As the pH increased above 7.1, however, we observed decomposition of PW_{11} into its original components, as evidenced by the decreasing signal at −11 ppm and the appearance of free phosphate at 2 ppm (Figure 3b). Decomposition of the parent PW_{12} anion into PW_{11} and WO_4 at neutral pH is represented in Figure 3c, and subsequent decomposition of PW_{11} into phosphate and tungstate is shown in Figure 3d. The assignments of ^{31}P NMR shifts were confirmed by electrospray ionization mass spectrometry studies at varying pH (Supplementary Figure S5, Supporting Information). With different sizes and charge densities, PW_{11} and WO_4 may each have distinct interactions with PrP and have different effects on the yield and purity of PrP^{Sc} obtained from PTA precipitation.

Effect of PTA-Derived Anions on PrP^{Sc} Precipitation. To measure the precipitation efficacy of each PTA component under physiological conditions, increasing concentrations of PW_{11}, WO_4, and mixtures thereof were used to precipitate PrP^{Sc} from brain homogenate. Brain homogenates from RML-infected FVB mice were incubated at 37 °C for 1 h with varying concentrations of POM solutions, ranging from 0.25 to 8 mM. POM stock solutions were made fresh by dissolving the following tungstates in water and adjusting the pH to 7.1: $Na_7[PW_{11}O_{39}]$, Na_2WO_4, a 1:1 mixture of PW_{11} and WO_4, and commercial NaPTA. Following incubation with the POM solutions, the brain samples were centrifuged at 14 000*g* for 1 h.[15,19] The supernatants were discarded, and PrP levels were measured in the pellets by enzyme-linked immunosorbent assay (ELISA) (Figure 4) or Western immunoblotting (Figure 5).

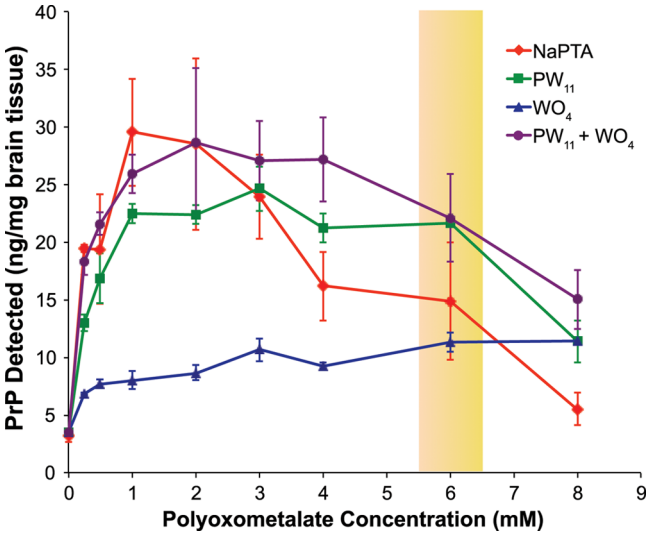

Figure 4. ELISA was used to quantify the amount of PrP precipitated from brain homogenates following incubation with varying concentrations of POMs. NaPTA (red), PW_{11} (green), and PW_{11} + WO_4 (purple) show a similar profile, whereas WO_4 (blue) appears to increase linearly in this concentration range. The yellow bar indicates the typical window of PTA concentrations used for PrP^{Sc} precipitations. Error bars represent the standard error of the mean across triplicate measurements of three independent sets of brain homogenate (7 brains/set).

Three independent sets of POM-precipitated samples were exposed to highly denaturing conditions (4 M guanidine hydrochloride at 100 °C) and then subjected to a sandwich ELISA (Figure 4). Commercial NaPTA resulted in a steep rise in the levels of detectable PrP when the concentration was increased from 0 to 1 mM and decreased gradually for the higher concentrations up to 8 mM. This trend was also observed for PW_{11} and the 1:1 mixture of PW_{11} and WO_4. By comparison, only a modest increase in detectable PrP was observed for equivalent WO_4 concentrations, suggesting that PW_{11} may have greater contribution in the facile detection of PrP than WO_4 by this method. The enhancement of PrP detection using POMs at different concentrations can also be expressed as a ratio of the observed values normalized to control samples where no POMs were used (Table 1). However, lipids have been shown to interfere with the detection of cholesterol, proteins, and other biomolecules by ELISA.[45−47] Indeed, several studies have shown that lipids can obscure the detection of PrP^{Sc} by ELISA in blood[32,48] and tissue homogenates.[49]

We performed Western immunoblotting to determine the relative level of PrP enrichment achieved by each PTA

DOI: 10.1021/cb5006239
ACS Chem. Biol. 2015, 10, 1269−1277

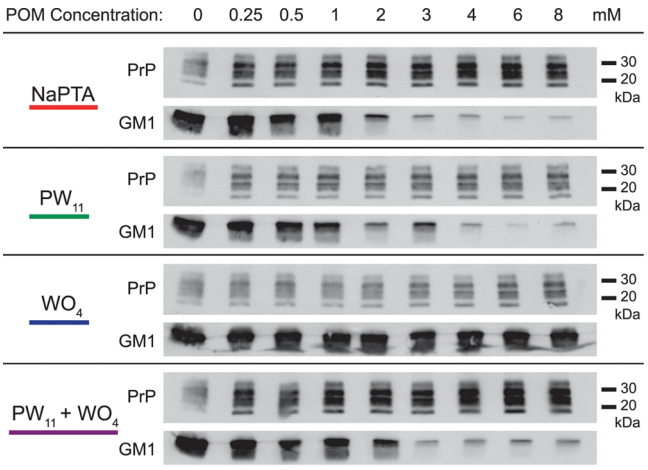

Figure 5. Immunoblots show the amounts of PrP and ganglioside GM1 in brain homogenates following incubation with different concentrations (0–8 mM) of POMs, as indicated. From top to bottom, POMs were sodium phosphotungstate (NaPTA), $Na_7[PW_{11}O_{39}]$ (PW_{11}), $Na_2[WO_4]$ (WO_4), and PW_{11} + WO_4. Molecular weight markers of migrated protein standards are shown in kilodaltons (kDa).

Table 1. Relative Enrichment of PrP Levels at Different Concentrations of POMs[a]

POM concn (mM)	PTA	PW_{11}	WO_4	PW_{11} + WO_4
0	1.0 ± 0.2	1.0 ± 0.2	1.0 ± 0.2	1.0 ± 0.2
0.25	6.1 ± 0.1	4.1 ± 0.3	2.1 ± 0.1	5.8 ± 0.4
0.5	6.1 ± 1.5	5.3 ± 0.7	2.4 ± 0.2	6.8 ± 0.3
1	9.3 ± 1.5	7.1 ± 0.3	2.5 ± 0.3	8.1 ± 0.6
2	9.0 ± 2.4	7.0 ± 0.3	2.7 ± 0.2	9.0 ± 2.1
3	7.5 ± 1.2	7.7 ± 0.6	3.4 ± 0.3	8.5 ± 1.1
4	5.1 ± 1.0	6.7 ± 0.4	2.9 ± 0.1	8.5 ± 1.2
6	4.7 ± 1.6	6.8 ± 0.1	3.6 ± 0.3	6.9 ± 1.2
8	1.7 ± 0.5	3.6 ± 0.6	3.6 ± 0.1	4.7 ± 0.8

[a]Compared with PrP levels without precipitant, as detected by ELISA.

component using the D13 antibody conjugated to horseradish peroxidase (HRP);[50] GM1 levels were also probed using the HRP-coupled cholera toxin B subunit, which specifically recognizes the ganglioside GM1 (Figure 5). GM1 is the predominant ganglioside in neuronal membranes and is often used as marker for lipid rafts.[51,52] While other raft lipids such as cholesterol were not measured directly, the detection of GM1 with cholera toxin-based reagents is straightforward, and the presence of GM1 can be used as an indicator for the general distribution of neuronal lipids in relation to PrP.

At concentrations from 0.25 to 8 mM, NaPTA and the 1:1 mixture of PW_{11} and WO_4 showed similar levels of PrP, in agreement with the decomposition of the parent PW_{12} ion into PW_{11} and WO_4 at physiological pH. Analysis of these POMs alone revealed that both PW_{11} and WO_4 contributed to the precipitation efficiency of PTA solutions. However, the separation of lipids from PrP^{Sc} differed substantially for each PTA component at equimolar concentrations. PW_{11} at concentrations >1 mM resulted in a substantial decrease in GM1 levels, whereas WO_4 did not affect GM1 levels. These results suggest that while both PTA components contribute to the precipitation of PrP, PW_{11} may be more effective in disrupting the interaction between PrP and lipids such as GM1, thereby increasing the relative purity of the precipitates.

Comparing the results from the ELISAs and Western blots, the discrepancy in the levels of PrP measured by these two methods at very low concentrations of POM likely results from the presence of GM1, and perhaps other lipids, associated with PrP. In cases where sensitivity of PrP^{Sc} detection is crucial, it is therefore important to use high enough concentrations of PTA (or PW_{11} in particular) to reduce the amount of coprecipitating lipids and facilitate detection of PrP^{Sc} in blood and tissue samples for diagnostic purposes.

CONCLUSIONS

Using spectrochemical, biophysical, and microscopic techniques, we observed that the effective precipitation of PrP^{Sc} by PTA may occur by some combination of facilitated fibril formation, enhanced separation of lipids from PrP^{Sc}, and increased density of PrP^{Sc} aggregates. The increase in the amount of large aggregates obtained when PTA and sarkosyl were used together (Figure 1) suggests that the separation of lipids such as GM1 from PrP^{Sc} is a major factor that can influence prion precipitation. It is possible that the observed fibrillization is a direct consequence of lipid removal by PTA and sarkosyl, since PrP^{Sc} detached from membranes readily forms amyloid.[39] Additionally, ganglioside GM1, the most abundant neuronal ganglioside,[35] was also studied as a marker of total lipid content and an indicator of sample purity. We found decreased levels of GM1 with higher concentrations of NaPTA, PW_{11} + WO_4, and PW_{11} while WO_4 was not as effective at equimolar concentrations (Figure 5).

From sucrose cushion centrifugations, incubation with PTA increased the density of PrP aggregates (Figure 2). PrP^{Sc} alone has a density of approximately 1.35 g/mL, while an 80% sucrose solution has a density of ∼1.41 g/mL.[53] The PrP aggregates that permeated the 80% sucrose cushion and formed the pellet must have a density in excess of 1.41 g/mL.

Unlike most proteins, PrP has a high isoelectric point of approximately 9 for the full-length protein,[54] rendering the protein positively charged at neutral pH. This feature of PrP may be used advantageously because manipulation of electrostatic interactions can be achieved using anionic compounds such as PTA and detergents. Our work on the pH-dependent decomposition of polyoxometalates (Figure 3) suggests that PrP^{Sc} precipitations using PTA should be carried out on the lower end of the physiological pH range, closer to pH 7.1 rather than 7.4, in order to maintain the integrity of the PW_{11} ion, particularly when greater sample purity is desired.

While both PW_{11} and WO_4 components of PTA contributed to the yield of PrP during precipitation, PW_{11} is primarily responsible for a reduction in coprecipitating GM1 lipids, as evidenced by the levels of ganglioside GM1 by Western blot (Figure 5). PW_{11} at concentrations >1 mM substantially reduced the level of coprecipitating lipids, while WO_4 did not at equivalent concentrations. This lipid reduction might explain why precipitation with PW_{11} facilitated detection of PrP by ELISA more effectively than the WO_4 component at concentrations between 0.25 and 6 mM (Figure 4). The lipids remaining in the WO_4-incubated samples may mask epitopes on PrP and hinder its binding to the detection antibodies in ELISA. The difference in lipid levels following PW_{11} and WO_4 precipitations may be attributed to the size and charge differences between the two tungstates, because the WO_4 ion has a single heavy tungsten atom and a delocalized −2 charge while PW_{11} is a much larger, heavier anion with a −7 charge. These differences between PW_{11} and WO_4 as well as our

DOI: 10.1021/cb5006239
ACS Chem. Biol. 2015, 10, 1269–1277

experiments with NaCl indicate that electrostatic interactions may be involved in promoting PrP^{Sc} precipitation by their disruption of interactions between PrP^{Sc} and buoyant anionic lipids like GM1. Direct association of dense tungstates with positively charged PrP^{Sc} may also contribute to the precipitation efficiency.

Reducing the amount of coprecipitating lipids such as GM1 may have implications for various areas of prion research, including biophysical studies of protein structure and diagnostic assay development. Lipids have been shown to interfere with protein detection assays, particularly those relying on the specificity of a protein−antibody interaction.[32,48] By reducing the lipid content of biological samples with typically low prion titers, high-throughput detection assays for cattle and human blood may be developed to reduce the risk of contracting variant Creutzfeldt−Jakob disease from meat products or blood transfusions.

By elucidating the mechanisms of PTA precipitation of PrP^{Sc}, we can improve our methods for sample preparation, which may play a crucial role in studies to probe the structure of PrP^{Sc} and to develop robust diagnostic tools. The principles governing the precipitation of PrP^{Sc} may also prove useful in studying other protein-misfolding diseases, in which the hydrophobic nature of protein aggregates promotes undesired binding of lipids to the aggregates.

METHODS

Chemicals. NaPTA, sodium tungstate dihydrate, sodium phosphate monobasic, sodium carbonate monobasic, *N*-laurylsarcosine sodium salt (sarkosyl), sucrose, cholera toxin subunit-B peroxidase conjugate, β-mercaptoethanol, trizma hydrochloride, sodium chloride, tween-20, sodium hydroxide, nitric acid, and hydrochloric acid were purchased from Sigma-Aldrich and used without further purification. Deuterium oxide was obtained from Cambridge Isotopes and used as received. Bovine serum albumin (BSA), ABTS substrate, and 8 M GdnHCl were obtained from Thermo Scientific. SDS, 10× TGS running buffer, and 10× Ca^{2+}/Mg^{2+}-free PBS were obtained from Gibco and diluted to the appropriate strength with purified water (18.2 MΩ·cm resistivity). Instant nonfat dry milk was from SACO Foods. Amersham enhanced chemiluminscence (ECL) Western blotting detection reagents were from GE Healthcare. Recombinant mouse PrP(23−230),[55] HRP-conjugated anti-PrP Fab antibody P,[56] and anti-PrP Fab antibodies D18 and HRP-D13[50] were prepared as described.

Prion-Infected Brain Samples. FVB weanling mice (Charles River Laboratories) were inoculated intracerebrally with RML prions prepared from infected CD1 mice. Inoculated mice were sacrificed when symptoms of neurologic dysfunction presented in accordance with protocols approved by the UCSF Institutional Animal Care and Use Committee. The brains were collected and stored at −80 °C. All manipulations of mice, brain tissue, and purified prions were performed in a Biosafety Level 2 facility in accordance with established guidelines from the NIH.

PrP Fibrillization Assays. Brain homogenates (10% w/v) were prepared in Ca^{2+}/Mg^{2+}-free PBS and clarified by centrifugation at 500*g* for 5 min in a tabletop centrifuge. The resulting supernatant was separated into 1-mL aliquots and centrifuged at 100 000*g* for 1 h (Beckman, TLA55 at 48 000 rpm). The high-speed supernatant was discarded, and the pellets remaining in the centrifuge tubes were frozen on ice and stored at −80 °C until use.

For the fibrillization assays, brain homogenate samples were resuspended with 200 μL of Ca^{2+}/Mg^{2+}-free PBS with Complete Protease Inhibitor Cocktail (Roche Applied Science, Indianapolis, IN) and then pooled together. The pooled samples were supplemented with increasing concentrations of PTA (0−3.4% w/v), sarkosyl (0−3.5% w/v), or a combination of PTA (0−3.4% w/v) in the presence of 2% w/v sarkosyl. The samples were incubated overnight (16−18 h) at 37 °C under constant shaking (1200 rpm). After incubation, the samples were place on ice, and 50-μL aliquots were taken and analyzed by electron microscopy.

Electron Microscopy. Sample aliquots of 5 μL were adsorbed for 30 s onto Formvar/carbon-coated, 200-mesh copper grids (Ted Pella, Redding, CA) that were glow-discharged prior to use. The grids were then washed briefly with 0.1 and 0.01 M ammonium acetate buffer, pH 7.4, and stained with two 50 μL drops of freshly filtered 2% w/v ammonium molybdate[57] or dried without additional staining. The contrast provided by the bound PTA was sufficient to identify fibrillization products at low magnification.[15] After drying, the samples were viewed with a FEI Tecnai F20 electron microscope (FEI Company, Hillsborough, OR) at an acceleration voltage of 80 kV. Electron micrographs were recorded on a Gatan (Pleasanton, CA) UltraScan 4000 CCD camera.

Fibril Quantification. The quantification of the PrP^{Sc} fibrillization was performed essentially as described.[15] In brief, 10 electron micrographs were taken at random positions on the grid. Micrographs that contained obvious film defects, dirt particles, and other artifacts were discarded and replaced. All images were taken at a low magnification of 7575× (corresponding to 19.8 Å/pixel) and a higher-than-usual underfocus (5−10 μm) to facilitate the quantification. The micrographs were processed with Adobe Photoshop (San Jose, CA). The number of pixels (representing the area) for each visible fibril in the electron micrographs was determined. Individual fibrils and fibril clusters were selected by using the magic wand tool with a setting of 50−100; the Fresnel fringes caused by the strong underfocus made it easier to delineate each fibril/fibril cluster separately. The histogram menu provided the number of pixels for each particle. Fibrils were classified as such if the length was >40 pixels, equivalent to ∼78 nm, and the length/width ratio was at least 2:1. The amount of fibrils was averaged over all 10 micrographs. The stochastic distribution of the fibrils on the support film is reflected in the relatively large standard errors of the mean (SEM).

Sucrose Cushion Centrifugations. Brain homogenate was prepared from RML-infected FVB mice at 20% w/v in Ca^{2+}/Mg^{2+}-free PBS. The homogenate was centrifuged for 5 min at 500*g* at 4 °C, and the pellet was discarded to remove cell debris from the sample. The supernatant was then split into two aliquots, and sarkosyl was added to each aliquot to give a final concentration of 2% w/v sarkosyl. To one sample, 10% PTA solution, pH 7.2, was added (2% final w/v), while the other was left as a control without PTA. The samples were then incubated overnight at 37 °C, and the aliquots were each pipetted onto a two-step sucrose cushion containing 50% sucrose (8 mL) and 80% sucrose layers (2 mL). All sucrose solutions contain 0.5% sarkosyl, 50 mM sodium HEPES, and 1 mM sodium azide. The gradients were centrifuged at 134 000*g* (20 °C) for 16 h in a SW41 Ti swinging bucket rotor (Beckman-Coulter). Fifteen aliquots were taken from each gradient and labeled A−O from low to high density. For fractions A−F, 1 mL samples were collected; for fractions G−O, 500 μL collected. The pellets were resuspended in 1 mL of a 2% sarkosyl solution and labeled as the pellet fraction. All aliquots and gradient pellet samples were analyzed by Western blot using the P-HRP antibody and developed using ECL reagents.

^{31}P Nuclear Magnetic Resonance. Samples were prepared at 10% w/v PTA in 90:10 H_2O/D_2O mixture and run on a Bruker Avance III NMR spectrometer equipped with a BBO broadband probe operating at 600.13 MHz for ^{1}H and 242.93 MHz for ^{31}P. Sample pH was adjusted with stepwise addition of NaOH and allowed to equilibrate for 1 h before spectra were collected. Additional spectra were collected in more complex buffer solutions containing PBS, sarkosyl, and brain homogenate (Supporting Information). While the phosphate concentration increased due to the use of PBS as the solvent, the NMR signals corresponding to PTA did not change in these complex buffer solutions.

Preparation of POM Stock Solutions. The 10% w/v (31.6 mM) PTA solutions were prepared by dissolution of NaPTA in deionized water (18.2 MΩ·cm resistivity); the pH of the solution was adjusted to pH 7.1−7.2 with NaOH. $Na_7[PW_{11}O_{39}]$ and $Na_2WO_4{\cdot}2H_2O$ solutions of equivalent concentrations (31.6 mM) were prepared in deionized

DOI: 10.1021/cb5006239
ACS Chem. Biol. 2015, 10, 1269−1277

water, and the pH was adjusted by NaOH or glacial acetic acid to pH 7.1−7.2. The solutions were prepared fresh prior to each experiment.

Synthesis of $Na_7[PW_{11}O_{39}]\cdot 12H_2O$. Procedure was adapted from Brevard et al.[58] Sodium tungstate dihydrate (36.3 g, 0.110 mol) and anhydrous sodium phosphate monobasic (1.38 g, 0.010 mol) were dissolved in 75 mL of deionized water (18.2 MΩ·cm resistivity). The solution was heated to 85−90 °C with vigorous stirring, and concentrated nitric acid was added dropwise to reach pH 4.8. The solution volume was reduced to half by evaporation, and extraction with 3 × 50 mL of acetone afforded the POM in the aqueous layer as a white powder after evaporation of the water.

Preparation of Brain Homogenates for Tungstate Precipitations. Triplicate sets of brain tissue (7 brains/set) from RML-infected FVB mice were thawed and homogenized with Ca^{2+}/Mg^{2+}-free PBS to give a 10% w/v crude brain homogenate. Nuclei and debris were removed by centrifugation at 1500*g* for 5 min, and the supernatant was diluted 1:1 with a sarkosyl detergent solution to a final concentration of 5% brain homogenate in 2% sarkosyl by weight. Samples were stored at −80 °C in 500-μL aliquots.

Tungstate Precipitations from Brain Homogenate. Aliquots (500-μL) of 5% brain homogenate in 2% sarkosyl (w/v) were treated with varying concentrations of tungstates by addition of 0, 8, 16, 32, 64, 96, 128, 192, or 256 μL of the stock solutions at pH 7.1 and a corresponding amount of water to adjust the final volume of each sample to 1012 μL. The samples were incubated at 37 °C with shaking for 1 h and then centrifuged at 14 000*g* for 1 h at room temperature (RT) in a 5415D Eppendorf microcentrifuge equipped with the fixed-angle rotor F-45-24-11. The supernatants were promptly decanted, and the 1.5 mL Eppendorf tubes were left upside-down to facilitate removal of liquid residue from the pellet, which was subsequently removed by cotton swabs. The pellets were stored at −20 °C.

ELISA Plate Preparation. Thermo Immulon 2HB flat-bottom, 96-well microtiter plates were used for ELISA experiments. To each well, 100 μL of 4 μg/mL solution of D18 antibody in 0.1 M carbonate (pH 8.6) was added, and the plates were sealed and incubated with shaking at 4 °C overnight. The plates were washed 5 times with Tris-buffered saline with Tween-20 (TBST) and then blocked with 300 μL/well of 1% BSA in TBST for 1 h at RT. After aspiration of the blocking solution, the plates were sealed and stored at 4 °C until use.

Sandwich ELISA. Three independently prepared sets of POM-precipitated pellets were resuspended in 500 μL of 4 M GdnHCl, heated at 100 °C for 10 min, and cooled on ice for 5 min. The samples were diluted 40-fold with 1% BSA in TBST to prevent antibody denaturation, and 100 μL of each sample was loaded onto D18-coated plates in triplicate. Each plate also contained a ladder of recombinant mouse PrP(23−230) loaded in known quantities in duplicate or triplicate to establish a standard concentration curve with a four-parameter logistic regression.[59] The plates were incubated overnight at 4 °C and subsequently washed 3× with TBST. The plates were then incubated for 1 h with a 1 μg/mL D13-HRP antibody solution in 1% BSA in PBS, rinsed 3× with TBST, and then developed with ABTS HRP substrate. Plate absorbance was read at 405 nm, and the sample optical densities were correlated to the known calibration curve to determine the level of PrP in each sample. To convert PrP levels from nanograms per well to nanograms per milligram of brain tissue, the well concentrations were multiplied by a factor of 8. The mean level of PrP precipitated at each POM concentration was calculated by taking the average of all samples at the same POM concentration, and the standard error of the mean was determined by taking the standard deviation of the independent averages and dividing by the square-root of three. To calculate the enrichment factor (eq 1) from each POM concentration relative to controls (Table 1), the values were normalized to the amount of PrP detected when no POMs were used in the precipitation.

$$\frac{\bar{x}_i}{\bar{x}_c} \pm \frac{\bar{x}_i}{\bar{x}_c}\sqrt{(\bar{x}_i - s_i)^2 + (\bar{x}_c - s_c)^2} \quad (1)$$

where $\bar{x}_i$ = average ng of PrP/mg of brain tissue for POM concentration *i*, $\bar{x}_c$ = average ng of PrP/mg of brain tissue for control (*i* = 0 mM POM), s_i = standard error of the mean for POM concentration *i*, and s_c = standard error of the mean for control (*i* = 0 mM POM).

Immunoblotting of POM-Precipitated Samples. POM-precipitated pellets were resuspended in 200 μL of SDS sample buffer, diluted 10-fold, heated to 100 °C for 10 min, and allowed to cool to RT. The samples were run on a BioRad Criterion 4−20% polyacrylamide gel, transferred to a PVDF membrane using the iBlot wet transfer system, blocked with a 5% milk solution in TBST, and incubated with 1 mg mL^{-1} D13-HRP antibody overnight at RT. To detect GM1, HRP-conjugated cholera toxin B subunit (Sigma-Aldrich) was added to the D13-HRP-containing milk solution the following day and incubated for 1 h at RT. The membrane was washed 3 times with TBST, incubated with ECL reagents for 1 min, and then developed on film.

■ ASSOCIATED CONTENT

Ⓢ Supporting Information

Additional sucrose cushion centrifugation studies and further characterization of PTA solutions by ^{31}P NMR and electrospray ionization mass spectrometry. This material is available free of charge via the Internet at http://pubs.acs.org.

■ AUTHOR INFORMATION

Corresponding Author

*jrlong@berkeley.edu.

Present Addresses

[⊥]J.O.: Department of Biophysics, Ruhr-Universität Bochum, Universitätsstraße 150, 44780 Bochum, Germany.

[∥]H.W.: Department of Biochemistry and Centre for Prions and Protein Folding Diseases, 204 Brain and Aging Research Building, University of Alberta, Edmonton, AB T6G 2M8, Canada.

Notes

The authors declare no competing financial interest.

■ ACKNOWLEDGMENTS

We thank the staff at the Hunter's Point Animal Facility for their assistance in providing tissue samples and A.T. Iavarone for assistance with mass spectrometry measurements. This work was sponsored by grants from the NIH (AG002132, AG021601, and AG010770) as well as by a gift from the Sherman Fairchild Foundation. D.J.L. was supported by the Department of Defense (DoD) through the National Defense Science & Engineering Graduate Fellowship (NDSEG) Program and the National Science Foundation Graduate Research Fellowship Program (NSF GRFP). We also thank the UC Berkeley NMR Facility (NIH Grant SRR023679A) and QB3/Chemistry Mass Spectrometry Facility for access to instrumentation.

■ REFERENCES

(1) Colby, D. W., and Prusiner, S. B. (2011) Prions. *Cold Spring Harbor Perspect. Biol.* 3, No. a006833.

(2) Prusiner, S. B. (2007) Prions, in *Fields Virology* (Knipe, D. M., Howley, P. M., Griffin, D. E., Lamb, R. A., Martin, M. A., Roizman, B., and Straus, S. E., Eds.) 5th ed., pp 3059−3092, Lippincott Williams & Wilkins, Philadelphia.

(3) Prusiner, S. B. (2012) A unifying role for prions in neurodegenerative diseases. *Science 336*, 1511−1513.

(4) Pan, K.-M., Baldwin, M., Nguyen, J., Gasset, M., Serban, A., Groth, D., Mehlhorn, I., Huang, Z., Fletterick, R. J., Cohen, F. E., and Prusiner, S. B. (1993) Conversion of α-helices into β-sheets features in the formation of the scrapie prion proteins. *Proc. Natl. Acad. Sci. U.S.A. 90*, 10962−10966.

DOI: 10.1021/cb5006239
ACS Chem. Biol. 2015, 10, 1269−1277

(5) Collinge, J., Palmer, M., Dryden, A., and Campbell, T. (1991) Molecular genetics of inherited, sporadic and iatrogenic prion disease, Presented at the Prion Diseases in Humans and Animals Conference, London, UK.
(6) Meyer-Luehmann, M., Coomaraswamy, J., Bolmont, T., Kaeser, S., Schaefer, C., Kilger, E., Neuenschwander, A., Abramowski, D., Frey, P., Jaton, A. L., Vigouret, J. M., Paganetti, P., Walsh, D. M., Mathews, P. M., Ghiso, J., Staufenbiel, M., Walker, L. C., and Jucker, M. (2006) Exogenous induction of cerebral beta-amyloidogenesis is governed by agent and host. *Science 313*, 1781−1784.
(7) Stöhr, J., Watts, J. C., Mensinger, Z. L., Oehler, A., Grillo, S. K., DeArmond, S. J., Prusiner, S. B., and Giles, K. (2012) Purified and synthetic Alzheimer's amyloid beta (Aβ) prions. *Proc. Natl. Acad. Sci. U.S.A. 109*, 11025−11030.
(8) Luk, K. C., Kehm, V. M., Zhang, B., O'Brien, P., Trojanowski, J. Q., and Lee, V. M. Y. (2012) Intracerebral inoculation of pathological α-synuclein initiates a rapidly progressive neurodegenerative α-synucleinopathy in mice. *J. Exp. Med. 209*, 975−986.
(9) Watts, J. C., Giles, K., Oehler, A., Middleton, L., Dexter, D. T., Gentleman, S. M., DeArmond, S. J., and Prusiner, S. B. (2013) Transmission of multiple system atrophy prions to transgenic mice. *Proc. Natl. Acad. Sci. U.S.A. 110*, 19555−19560.
(10) Clavaguera, F., Akatsu, H., Fraser, G., Crowther, R. A., Frank, S., Hench, J., Probst, A., Winkler, D. T., Reichwald, J., Staufenbiel, M., Ghetti, B., Goedert, M., and Tolnay, M. (2013) Brain homogenates from human tauopathies induce tau inclusions in mouse brain. *Proc. Natl. Acad. Sci. U.S.A. 110*, 9535−9540.
(11) Sanders, D. W., Kaufman, S. K., DeVos, S. L., Sharma, A. M., Mirbaha, H., Li, A., Barker, S. J., Foley, A. C., Thorpe, J. R., Serpell, L. C., Miller, T. M., Grinberg, L. T., Seeley, W. W., and Diamond, M. I. (2014) Distinct tau prion strains propagate in cells and mice and define different tauopathies. *Neuron 82*, 1−18.
(12) Wille, H., Bian, W., McDonald, M., Kendall, A., Colby, D. W., Bloch, L., Ollesch, J., Boronvinskiy, A. L., Cohen, F. E., Prusiner, S. B., and Stubbs, G. (2009) Natural and synthetic prion structure from X-ray fiber diffraction. *Proc. Natl. Acad. Sci. U.S.A. 106*, 16990−16995.
(13) Govaerts, C., Wille, H., Prusiner, S. B., and Cohen, F. E. (2004) Evidence for assembly of prions with left-handed β-helices into trimers. *Proc. Natl. Acad. Sci. U.S.A. 101*, 8342−8347.
(14) Smirnovas, V., Baron, G. S., Offerdahl, D. K., Raymond, G. J., Caughey, B., and Surewicz, W. K. (2011) Structural organization of brain-derived mammalian prions examined by hydrogen-deuterium exchange. *Nat. Struct. Mol. Biol. 18*, 504−506.
(15) Wille, H., Shanmugam, M., Murugesu, M., Ollesch, J., Stubbs, G., Long, J. R., Safar, J. G., and Prusiner, S. B. (2009) Surface charge of polyoxometalates modulates polymerization of the scrapie prion protein. *Proc. Natl. Acad. Sci. U.S.A. 106*, 3740−3745.
(16) Prusiner, S. B., McKinley, M. P., Bowman, K. A., Bolton, D. C., Bendheim, P. E., Groth, D. F., and Glenner, G. G. (1983) Scrapie prions aggregate to form amyloid-like birefringent rods. *Cell 35*, 349−358.
(17) McKinley, M. P., Bolton, D. C., and Prusiner, S. B. (1983) Fibril-like structures in preparations of scrapie prions purified from hamster brain. *Proc. - Electron Microsc. Soc. Am.*, 802−803.
(18) Sim, V. L., and Caughey, B. (2009) Ultrastructures and strain comparison of under-glycosylated scrapie prion fibrils. *Neurobiol. Aging 30*, 2031−2042.
(19) Safar, J., Wille, H., Itri, V., Groth, D., Serban, H., Torchia, M., Cohen, F. E., and Prusiner, S. B. (1998) Eight prion strains have PrP^{Sc} molecules with different conformations. *Nat. Med. 4*, 1157−1165.
(20) White, A. R., Enever, P., Tayebi, M., Mushens, R., Linehan, J., Brandner, S., Anstee, D., Collinge, J., and Hawke, S. (2003) Monoclonal antibodies inhibit prion replication and delay the development of prion disease. *Nature 422*, 80−83.
(21) Hill, A. F., Butterworth, R. J., Joiner, S., Jackson, G., Rossor, M. N., Thomas, D. J., Frosh, A., Tolley, N., Bell, J. E., Spencer, M., King, A., Al-Sarraj, S., Ironside, J. W., Lantos, P. L., and Collinge, J. (1999) Investigation of variant Creutzfeldt-Jakob disease and other human prion diseases with tonsil biopsy samples. *Lancet 353*, 183−189.
(22) Glatzel, M., Abela, E., Maissen, M., and Aguzzi, A. (2003) Extraneural pathologic prion protein in sporadic Creutzfeldt-Jakob disease. *N. Engl. J. Med. 349*, 1812−1820.
(23) Wroe, S. J., Pal, S., Siddique, D., Hyare, H., Macfarlane, R., Joiner, S., Linehan, J. M., Brandner, S., Wadsworth, J. D., Hewitt, P., and Collinge, J. (2006) Clinical presentation and pre-mortem diagnosis of variant Creutzfeldt-Jakob disease associated with blood transfusion: A case report. *Lancet 368*, 2061−2067.
(24) Saa, P., Castilla, J., and Soto, C. (2006) Ultra-efficient replication of infectious prions by automated protein misfolding cyclic amplification. *J. Biol. Chem. 281*, 35245−35252.
(25) Huang, H., Rendulich, J., Stevenson, D., O'Rourke, K., and Balachandran, A. (2005) Evaluation of Western blotting methods using samples with or without sodium phosphotungstic acid precipitation for diagnosis of scrapie and chronic wasting disease. *Can. J. Vet. Res. 69*, 193−199.
(26) Lee, I. S., Long, J. R., Prusiner, S. B., and Safar, J. G. (2005) Selective precipitation of prions by polyoxometalate complexes. *J. Am. Chem. Soc. 127*, 13802−13803.
(27) Reichel, A. (2006) The role of blood-brain barrier studies in the pharmaceutical industry. *Curr. Drug Metab. 7*, 183−203.
(28) Colby, D. W., Zhang, Q., Wang, S., Groth, D., Legname, G., Riesner, D., and Prusiner, S. B. (2007) Prion detection by an amyloid seeding assay. *Proc. Natl. Acad. Sci. U.S.A. 104*, 20914−20919.
(29) Bennion, B. J., and Daggett, V. (2002) Protein conformation and diagnostic tests: The prion protein. *Clin. Chem. 48*, 2105−2114.
(30) Birkmann, E., Henke, F., Funke, S. A., Bannach, O., Riesner, D., and Willbold, D. (2008) A highly sensitive diagnostic assay for aggregate-related diseases, including prion diseases and Alzheimer's disease. *Rejuvenation Res. 11*, 359−363.
(31) Wadsworth, J. D., Joiner, S., Hill, A. F., Campbell, T. A., Desbruslais, M., Luthert, P. J., and Collinge, J. (2001) Tissue distribution of protease resistant prion protein in variant Creutz-feldt-Jakob disease using a highly sensitive immunoblotting assay. *Lancet 358*, 171−180.
(32) Bannach, O., Birkmann, E., Reinartz, E., Jaeger, K. E., Langeveld, J. P., Rohwer, R. G., Gregori, L., Terry, L. A., Willbold, D., and Riesner, D. (2012) Detection of prion protein particles in blood plasma of scrapie infected sheep. *PLoS One 7*, No. e36620.
(33) Godsave, S. F., Wille, H., Pierson, J., Prusiner, S. B., and Peters, P. J. (2013) Plasma membrane invaginations containing clusters of full-length PrP^{Sc} are an early form of prion-associated neuropathology. *Neurobiol. Aging 34*, 1621−1631.
(34) Sanghera, N., Correia, B. E., Correia, J. R., Ludwig, C., Agarwal, S., Nakamura, H. K., Kuwata, K., Samain, E., Gill, A. C., Bonev, B. B., and Pinheiro, T. J. (2011) Deciphering the molecular details for the binding of the prion protein to main ganglioside GM1 of neuronal membranes. *Chem. Biol. 18*, 1422−1431.
(35) Pang, H., Le, P. U., and Nabi, I. R. (2004) Ganglioside GM1 levels are a determinant of the extent of caveolae/raft-dependent endocytosis of cholera toxin to the Golgi apparatus. *J. Cell Sci. 117*, 1421−1430.
(36) Vey, M., Pilkuhn, S., Wille, H., Nixon, R., DeArmond, S. J., Smart, E. J., Anderson, R. G., Taraboulos, A., and Prusiner, S. B. (1996) Subcellular colocalization of the cellular and scrapie prion proteins in caveolae-like membranous domains. *Proc. Natl. Acad. Sci. U.S.A. 93*, 14945−14949.
(37) Stahl, N., Baldwin, M. A., Burlingame, A. L., and Prusiner, S. B. (1990) Identification of glycoinositol phospholipid linked and truncated forms of the scrapie prion protein. *Biochemistry 29*, 8879−8884.
(38) Elfrink, K., Ollesch, J., Stöhr, J., Willbold, D., Riesner, D., and Gerwert, K. (2008) Structural changes of membrane-anchored native PrP^{C}. *Proc. Natl. Acad. Sci. U.S.A. 105*, 10815−10819.
(39) Chesebro, B., Trifilo, M., Race, R., Meade-White, K., Teng, C., LaCasse, R., Raymond, L., Favara, C., Baron, G., Priola, S., Caughey, B., Masliah, E., and Oldstone, M. (2005) Anchorless prion protein results in infectious amyloid disease without clinical scrapie. *Science 308*, 1435−1439.

DOI: 10.1021/cb5006239
ACS Chem. Biol. 2015, 10, 1269−1277

(40) Stöhr, J., Watts, J. C., Legname, G., Oehler, A., Lemus, A., Nguyen, H.-O. B., Sussman, J., Wille, H., DeArmond, S. J., Prusiner, S. B., and Giles, K. (2011) Spontaneous generation of anchorless prions in transgenic mice. *Proc. Natl. Acad. Sci. U.S.A. 108*, 21223−21228.
(41) Keggin (1933) Structure of the molecule of 12-phosphotungstic acid. *Nature 131*, 908−909.
(42) Kyle, J. H. (1983) Kinetics of the base decomposition of dodecatungstophosphate(3-) in weakly alkaline solutions. *J. Chem. Soc., Dalton Trans.*, 2609−2612.
(43) Zhu, Z., Tain, R., and Rhodes, C. (2003) A study of the decomposition behaviour of 12-tungstophosphate heteropolyacid in solution. *Can. J. Chem. 81*, 1044−1050.
(44) Smith, B. J., and Patrick, V. A. (2004) Quantitative determination of aqueous dodecatungstophosphoric acid speciation by NMR spectroscopy. *Aust. J. Chem. 57*, 261−268.
(45) Zhang, W., Purchio, A. F., Coffee, R., and West, D. B. (2004) Differential regulation of the human CYP3A4 promoter in transgenic mice and rats. *Drug Metab. Dispos. 32*, 163−167.
(46) Ji, J. Z., and Meng, Q. H. (2011) Evaluation of the interference of hemoglobin, bilirubin, and lipids on Roche Cobas 6000 assays. *Clin. Chim. Acta 412*, 1550−1553.
(47) Lovering, F., Bikker, J., and Humblet, C. (2009) Escape from flatland: Increasing saturation as an approach to improving clinical success. *J. Med. Chem. 52*, 6752−6756.
(48) Edgeworth, J. A., Farmer, M., Sicilia, A., Tavares, P., Beck, J., Campbell, T., Lowe, J., Mead, S., Rudge, P., Collinge, J., and Jackson, G. S. (2011) Detection of prion infection in variant Creutzfeldt-Jakob disease: A blood-based assay. *Lancet 377*, 487−493.
(49) Baldrick, P. (2008) Safety evaluation to support First-In-Man investigations II: Toxicology studies. *Regul. Toxicol. Pharmacol. 51*, 237−243.
(50) Williamson, R. A., Peretz, D., Pinilla, C., Ball, H., Bastidas, R. B., Rozenshteyn, R., Houghten, R. A., Prusiner, S. B., and Burton, D. R. (1998) Mapping the prion protein using recombinant antibodies. *J. Virol. 72*, 9413−9418.
(51) Blank, N., Gabler, C., Schiller, M., Kriegel, M., Kalden, J. R., and Lorenz, H. M. (2002) A fast, simple and sensitive method for the detection and quantification of detergent-resistant membranes. *J. Immunol. Methods 271*, 25−35.
(52) Botto, L., Cunati, D., Coco, S., Sesana, S., Bulbarelli, A., Biasini, E., Colombo, L., Negro, A., Chiesa, R., Masserini, M., and Palestini, P. (2014) Role of lipid rafts and GM1 in the segregation and processing of prion protein. *PLoS One 9*, No. e98344.
(53) Reiser, P., Birch, G. G., and Mathlouthi, M. (1995) Physical properties, in *Sucrose: Properties and Applications* (Mathlouthi, M., and Reiser, P., Eds.), pp 186−222, Chapman & Hall, Glasgow.
(54) Morillas, M., Swietnicki, W., Gambetti, P., and Surewicz, W. K. (1999) Membrane environment alters the conformational structure of the recombinant human prion protein. *J. Biol. Chem. 274*, 36859−36865.
(55) Bocharova, O. V., Breydo, L., Parfenov, A. S., Salnikov, V. V., and Baskakov, I. V. (2005) In vitro conversion of full-length mammalian prion protein produces amyloid form with physical properties of PrP^{Sc}. *J. Mol. Biol. 346*, 645−659.
(56) Safar, J. G., Scott, M., Monaghan, J., Deering, C., Didorenko, S., Vergara, J., Ball, H., Legname, G., Leclerc, E., Solforosi, L., Serban, H., Groth, D., Burton, D. R., Prusiner, S. B., and Williamson, R. A. (2002) Measuring prions causing bovine spongiform encephalopathy or chronic wasting disease by immunoassays and transgenic mice. *Nat. Biotechnol. 20*, 1147−1150.
(57) Wille, H., and Prusiner, S. B. (1999) Ultrastructural studies on scrapie prion protein crystals obtained from reverse micellar solutions. *Biophys. J. 76*, 1048−1062.
(58) Brevard, C., Schimpf, R., Tourne, G., and Tourne, C. M. (1983) Tungsten-183 NMR: A complete and unequivocal assignment of the tungsten-tungsten connectivities in heteropolytungstates via two-dimensional tungsten-183 NMR techniques. *J. Am. Chem. Soc. 105*, 7059−7063.
(59) Leading Technology Group Pty Ltd. (2014) ElisaAnalysis (v. 3.2), Elisakit.com Pty Ltd., Victoria, Australia.
(60) Fuchs, J., Thiele, A., and Palm, R. (1981) Struktur und Schwingungsspektrum des α-UndekawolframatophosphatsNa$_2$ [N-(CH$_3$)$_4$]$_4$HPW$_{11}$O$_{39}$·7H$_2$O. *Z. Naturforsch. B 36*, 544−550.
(61) Okada, K., Morikawa, H., Marumo, F., and Iwai, S. (1974) Sodium tungstate. *Acta Crystallogr. B30*, 1872−1873.

DOI: 10.1021/cb5006239
ACS Chem. Biol. 2015, 10, 1269−1277